Optical absorption spectra of a quantum dot in a microcavity

1999 J. Phys.: Condens. Matter 11 6287

(http://iopscience.iop.org/0953-8984/11/32/319)

J. Phys.: Condens. Matter **11** (1999) 6287–6300. Printed in the UK PII: S0953-8984(99)01321-1

Optical absorption spectra of a quantum dot in a microcavity

J Thomas Andrews†, Pratima Sen† and Ravindra R Puri‡

† Department of Applied Physics, Shri G S Institute of Technology and Science, Indore 452003, India

‡ Theoretical Physics Division, Bhabha Atomic Research Centre, Mumbai 400 085, India

E-mail: pratima_sen@hotmail.com

Received 25 January 1999, in final form 17 May 1999

Abstract. Exact quantum electrodynamical results are obtained for a semiconductor quantum dot placed inside a microcavity of arbitrary photon leakage (κ), and radiative (γ) and nonradiative (γ_c) decay rates. Analytical results are obtained for the density matrix elements. The absorption spectra thus obtained for arbitrary values of κ, γ and γ_c exhibit the solid-state analogue of the vacuum Rabi splitting when the system decay parameters are much smaller than the quantum dot–cavity-field coupling parameter. Numerical estimates are made for samples of CdS and GaAs quantum dots of dimensions 19 Å and 56 Å, respectively. The results are in qualitative agreement with the experimental observations.

1. Introduction

Modern photolithographic and etching techniques have made it possible to realize microcavities in condensed matter systems [1]. At low excitation energy, a semiconductor microresonator will be occupied by less than one photon, leading to spontaneous emission due to electronic transitions from conduction to valence band states. This situation can be compared with that of an atom placed in a microcavity where the cavity size is comparable to the photon wavelength [2, 3]. There has been growing interest in recent years in the study of the solid-state analogue of the quantum effect of vacuum Rabi splitting [4–6]. Observation of the Rabi splitting in solids requires an equivalence of atomic and photon oscillators in monolithic semiconductor structures. It is well known that the oscillator strength of the electron–hole continuum in the volume of the exciton is concentrated at the excitonic energy, making it equivalent to a two-level atomic system [7].

In the case of quantum confined structures such as zero-dimensional quantum dots (QDs), the discrete energy spectrum of the QD exhibits a closer analogy with that of the atom. Time-resolved photoluminescence spectroscopy of CdS and GaAs quantum dots reveals distinct narrow lines [8]. For experimental purposes, the quantum dots are generally etched from two-dimensional quantum well structures. The Fabry–Pérot cavity grown by the metal–organic chemical vapour deposition (MOCVD) technique yields cavity mirrors with reflectivities of about 98%, which may be treated as the strong-coupling limit (SCL) for the QD and the electromagnetic radiation [4, 9]. For semiconductors, very fine microcavities can be realized by using distributed Bragg reflectors with embedded quantum wells. Lyngnes *et al* [10] used a $3\lambda/2$ GaAs spacer between a 14-period top and 16.5-period bottom GaAs/GaAlAs Bragg mirror having reflectivity $\approx$99.6%. For uncoated resonator faces of GaAs samples, the calculated reflectivities are $\approx$30%, since the refractive index of the semiconductor is about 3.5 times larger

0953-8984/99/326287+14$30.00

than the value unity outside [11]. Such cavities give rise to the so-called weak coupling of the QD with the cavity electromagnetic field. For such weak-coupling limits (WCL), irreversible decay of the population occurs, while for the SCL, the alternating absorption and emission of the cavity field leads to Rabi oscillations in the transmitted intensity and Rabi splitting in the frequency spectrum [8].

In the quantum mechanical description of a QD, one is required to take into account the role of (i) one- and two-electron–hole-pair (EHP) states, (ii) the Coulombic interaction energy and the (iii) confinement energy [12, 13]. At low excitation intensities and moderate temperatures, the exciton density is small and hence the contribution of 2-EHP states is negligible [14]. It has been shown that for a small QD of radius R smaller than the bulk excitonic Bohr radius ($R \leqslant a_B$), the confinement-induced energy shift is much larger than the Coulomb interaction energy, and one can safely ignore the Coulomb interaction without losing much accuracy [15]. However, the above-mentioned approximations are valid as long as one is not particularly concerned with calculating the exact wavefunctions and energy eigenfunctions of the system [16]. The optical properties of a small QD are highly sensitive to the sizes of the distributions of the QDs in an array. The variation of the QD size distribution can be accounted for by introducing a probability size distribution function. A spherical shape for the QD and the Gaussian distribution function for its radii have been proposed by Wu *et al* [17] while studying the average absorption of a QD in a quantum dot ensemble.

Of late, there has been growing interest in examining the role of so-called Coulomb blockade in semiconductor quantum dots at very low temperatures [18–23]. It is evident that tunnelling due to Coulomb blockade in semiconductor quantum dots such as GaAs/GaAlAs QDs can be significant only for electrostatic energy

$$\Delta E \approx e^2/C \gg k_B T$$

with C being the capacitance of the quantum dot [19]. It can easily be established by calculation that the photon-assisted tunnelling in the presence of Coulomb blockade is meaningful only in the recently developed area of microwave spectroscopy with very low excitation intensity [20]. In the present analysis we have considered photon excitation energy $\overline{h}\omega \approx \overline{h}\omega_g$ (=1.514 eV, $\overline{h}\omega_g$ being the band-gap energy), which is about 10^4 times larger than the Coulomb energy ($\Delta E \approx 0.16$ meV), as obtainable in a QD of GaAs [19]. The situation will be more or less unchanged for CdS. Accordingly, we have neglected the role of Coulomb blockade in the study of optical properties in semiconductor quantum dots subjected to optical radiation in the near-visible spectrum.

In the present paper, we have theoretically analysed the emission and absorption spectrum of a small quantum dot ($R \leqslant a_B$) placed in a microcavity, taking into account the role of single-EHP states below the semiconductor band edge. It is expected that the transition probability will be maximum for the resonant transitions, while it will decrease sharply with increasing departure from resonance. We have chosen a pump energy near the resonance for the lowest excitonic state. Taking into account the maximum frequency spread of a subpicosecond pulse (10^{14} s^{-1}), the quantum numbers for single-EHP states are restricted to $n = 1, 2$ and $l = 0, 1$. Accordingly, the direct allowed photo-induced electronic transitions to the excitonic states with $n = 1, 2$ and $l = 0, 1$ have been considered in the present model. We have incorporated the various decay parameters arising due to the cavity photon leakage (κ), and radiative (γ) and nonradiative (γ_c) decay rates. In order to analyse the optical properties of a QD in an array, we have used the Gaussian size distribution function. The present analysis has been applied to the specific cases of GaAs and CdS quantum dots of dimensions 56 Å and 19 Å, respectively, placed inside a microcavity of arbitrary Q-factor.

2. The model

We consider the interaction of quantized radiation with the quantum dot placed in a microcavity of arbitrary Q. The cavity supports a single mode of frequency ω and photons leak out at a rate of 2κ. The present formulations are constructed for a small quantum dot of size $R \leqslant a_B$, smaller than the bulk excitonic Bohr radius. Such smallness of the QD allows one to ignore the electron–hole (e–h) Coulombic energy in comparison to the exciton confinement energy [13]. This approximation is valid as long as one is not concerned with direct calculations of the energy difference or details of the electron–hole wavefunctions. We have also neglected the biexciton contribution, assuming the excitation intensity to be low enough to produce a large electron–hole pair density.

The total Hamiltonian for radiation–QD interaction can be defined as [13]

$$H = \sum_e \omega_e \pi_{ee} + \omega a^\dagger a + \sum_e g_e (a^\dagger \pi_{0e} + \text{h.c.}). \tag{1}$$

Here, ω is the pump frequency and $\hbar\omega_e$ $(=\hbar\omega_g - E_R(\alpha_e a_B/R)^2)$ is the energy of the eth exciton, E_R being the exciton Rydberg energy. $e = \{n, l\}$, with n, l the quantum numbers corresponding to the 1s, 1p, 1d, ..., 2s, 2p, ... levels of the electrons and holes. The parameter $g_e(=(\mu_e E)/\hbar)$ couples the eth exciton of the QD with the single mode of the cavity electromagnetic field, μ_e being the exciton transition dipole moment for the eth energy state. $a^\dagger$ and a are the creation and annihilation operators of the cavity field and $\pi_{ij} = |i\rangle\langle j|$. Consequently, the density matrix equation of motion can be written as

$$\frac{\partial \rho}{\partial t} = -\mathrm{i}[H, \rho] + \kappa L_c \rho + \gamma L_r \rho + \gamma_c L_{nr} \rho \equiv L\rho \tag{2}$$

where

$$L_c \rho = 2a\rho a^\dagger - a^\dagger a \rho - \rho a^\dagger a \tag{3}$$

$$L_r \rho = 2\pi_{0e} \rho \pi_{0e}^\dagger - \pi_{0e}^\dagger \pi_{0e} \rho - \rho \pi_{0e}^\dagger \pi_{0e} \tag{4}$$

$$L_{nr} \rho = 2\pi_{ee} \rho \pi_{ee} - \pi_{ee}^2 \rho - \rho \pi_{ee}^2. \tag{5}$$

Such an approach for incorporating the damping rates has been widely used by many authors in studying the interaction of a semiconductor with the single mode of the cavity field [9, 24, 25].

In obtaining (1)–(5) we assume that the cavity field has $n+1$ photons and the semiconductor contains no excitons, which is represented by $|n+1, 0\rangle$. With the loss of a photon, the QD acquires an exciton in any eth state represented by $|n, e\rangle$. The different excitonic states ($|0\rangle$ and $|e\rangle$) and the number of photons n in the cavity mode suggest $2n+1$ as the number of possible states. Hence, one has to deal with $(2n+1)^2 \times (2n+1)^2$ matrices to solve the density matrix equation (2). The trivial mathematics may be avoided by considering the initial state of the system as $|\emptyset, e\rangle$, which will return to either the $|1, 0\rangle$ rate or the $|\emptyset, 0\rangle$ state by radiative or nonradiative decay processes. In the forthcoming discussions, we have denoted the 'zeros' of the photon and exciton states by $|\emptyset\rangle$ and $|0\rangle$, respectively. The density matrix equation for the state $|\emptyset, e\rangle$ is found to be

$$\left[\frac{\mathrm{d}}{\mathrm{d}t} - \mathrm{i}\begin{pmatrix} \omega + \Delta_e + \mathrm{i}\Gamma & g_e \\ g_e & \omega + \mathrm{i}\kappa \end{pmatrix}\right] \begin{pmatrix} \langle \emptyset, 0|\rho|\emptyset, e\rangle \\ \langle \emptyset, 0|\rho|1, 0\rangle \end{pmatrix} = 0 \tag{6}$$

where $\Delta_e = \omega_e - \omega$ and $\Gamma = \gamma + \gamma_c$. The density matrix equations of motion are obtained as

$$\left[\frac{\mathrm{d}}{\mathrm{d}t} + \begin{pmatrix} 2\Gamma & \mathrm{i}g_e & -\mathrm{i}g_e & 0 \\ \mathrm{i}g_e & -(\mathrm{i}\Delta_e - \kappa - \Gamma) & 0 & -\mathrm{i}g_e \\ -\mathrm{i}g_e & 0 & \mathrm{i}\Delta_e + \kappa + \Gamma & \mathrm{i}g_e \\ 0 & -\mathrm{i}g_e & \mathrm{i}g_e & 2\kappa \end{pmatrix}\right] \begin{pmatrix} \langle \emptyset, e|\rho|\emptyset, e\rangle \\ \langle 1, 0|\rho|\emptyset, e\rangle \\ \langle \emptyset, e|\rho|1, 0\rangle \\ \langle 1, 0|\rho|1, 0\rangle \end{pmatrix} = 0. \tag{7}$$

The total ρ_{0e} can be calculated by summing over all of the electron–hole pair states existing from $|0\rangle$ to $|e\rangle$. Equations (6) can be used to study the emission and absorption characteristics while equation (7) yields the probability distribution. We first confine our attention to studying the probability distribution. Accordingly, using the Laplace transform technique [26], we get

$$\langle \emptyset, 0|\rho\big|\emptyset, e\rangle = \frac{1}{r_e^+ - r_e^-}\Big[\big[(r_e^+ - \mathrm{i}\omega + \kappa)\langle \emptyset, 0|\rho(0)\big|\emptyset, e\rangle + \mathrm{i}g_e\langle \emptyset, 0|\rho(0)\big|1, 0\rangle\big]\,\mathrm{e}^{r_e^+ t} - \big[(r_e^- - \mathrm{i}\omega + \kappa)\langle \emptyset, 0|\rho(0)\big|\emptyset, e\rangle + \mathrm{i}g_e\langle \emptyset, 0|\rho(0)\big|1, 0\rangle\big]\,\mathrm{e}^{r_e^- t}\Big] \tag{8}$$

and

$$\langle \emptyset, 0|\rho\big|1, 0\rangle = \frac{1}{r_e^+ - r_e^-}\Big[\big[[r_e^+ - \mathrm{i}(\omega + \Delta_e) + \Gamma]\langle \emptyset, 0|\rho(0)\big|1, 0\rangle + \mathrm{i}g_e\langle \emptyset, 0|\rho(0)\big|\emptyset, e\rangle\big]\,\mathrm{e}^{r_e^+ t} - \big[[r_e^- - \mathrm{i}(\omega + \Delta_e) + \kappa]\langle \emptyset, 0|\rho(0)\big|1, 0\rangle + \mathrm{i}g_e\langle \emptyset, 0|\rho(0)\big|\emptyset, e\rangle\big]\,\mathrm{e}^{r_e^- t}\Big] \tag{9}$$

with

$$r_e^{\pm} = \mathrm{i}\left(\omega + \frac{\Delta_e}{2}\right) - \frac{\kappa + \Gamma}{2} \pm \frac{1}{2}[(\mathrm{i}\Delta_e + \kappa - \Gamma)^2 - 4g_e^2]^{1/2}. \tag{10}$$

Similarly, the solutions for the Laplace-transformed variables are found from

$$\begin{pmatrix} \hat{\varphi}_1(r) \\ \hat{\varphi}_2(r) \\ \hat{\varphi}_3(r) \\ \hat{\varphi}_4(r) \end{pmatrix} = \frac{M}{A(r)} \begin{pmatrix} \hat{\varphi}_1(0) \\ \hat{\varphi}_2(0) \\ \hat{\varphi}_3(0) \\ \hat{\varphi}_4(0) \end{pmatrix} \tag{11}$$

where

$$M = \begin{pmatrix} 4g^2 r_1 + r_0[r_1^2 - (\kappa - \Gamma)^2] & \mathrm{i}\Delta_e r_2^2 & 2g_e\Delta_e(\kappa - \Gamma) & 2g_e\Delta_e r_1 \\ \mathrm{i}\Delta_e r_2^2 & r_0 r_2^2 & -2\mathrm{i}g_e r_0(\kappa - \Gamma) & -2\mathrm{i}g_e r_0 r_1 \\ 2g_e\Delta_e(\kappa - \Gamma) & -2\mathrm{i}g_e r_0(\kappa - \Gamma) & r_1 r_3^2 + 4r_0 g_e^2 & r_3^2(\kappa - \Gamma) \\ 2g_e\Delta_e\Gamma & -2\mathrm{i}g_e r_0 r_1 & r_3^2(\kappa - \Gamma) & r_1 r_3^2 \end{pmatrix}$$

with $r_0 = r + \kappa + \Gamma$; $r_1 = r + \kappa + \gamma$; $r_2^2 = r_1^2 - (\kappa - \Gamma)^2$; $r_3^2 = r_0^2 + \Delta_e^2$ and also $\hat{\varphi}(r)_{1/2} = \langle 1, 0|\hat{\rho}\big|0, e\rangle \pm \langle \emptyset, e|\hat{\rho}\big|1, 0\rangle$ and $\hat{\varphi}(r)_{3/4} = \langle \emptyset, e|\hat{\rho}\big|\emptyset, e\rangle \pm \langle 1, 0|\hat{\rho}\big|1, 0\rangle$. The carets in (11) indicate the Laplace-transformed variables. The polynomial $A(r)$ is given by

$$A(r) = (r_0^2 + \Delta_e^2)[r_1^2 - (\kappa - \Gamma)^2] + 4g_e^2 r_0 r_1. \tag{12}$$

Usage of (11) and (12) yields $\langle 1, 0|\hat{\rho}\big|\emptyset, e\rangle$ as

$$\langle 1, 0|\hat{\rho}\big|\emptyset, e\rangle = -\frac{\mathrm{i}g_e}{A(r)}(r_0 + \mathrm{i}\Delta_e)(r_0 + \kappa - \Gamma). \tag{13}$$

In our forthcoming discussions, we have represented $\langle 1, 0|\rho\big|\emptyset, e\rangle$ as ρ_{0e}. Also, ρ_{0e} has been calculated for the damping parameters corresponding to the weak- and strong-coupling regimes of the small quantum dot. The present theoretical model is an extension of the work reported by Agarwal [25] developed to study electromagnetic results for scattering, emission and absorption from a Rydberg atom in a microcavity of arbitrary Q. Equations (11)–(13) can be reduced to those of Agarwal [25] if one neglects the excitonic effect and puts $\gamma = \gamma_c = 0$ in the present formulations. The coupling parameter g_e and the exciton–cavity detuning parameter Δ_e defined in the current analysis take into account the different excitonic states existing in the case of the quantum dots in the semiconductor.

The confinement effects in the QD cause a shift of the absorption lines to the higher-energy side. In an inhomogeneous distribution of QDs (IQD) the absorption line broadens

due to the presence of many QDs of varying sizes in the surroundings. For typical quantum dot samples grown in semiconductor-doped glasses or colloids, it is known that the dot sizes vary by 15–20% from the average dot size. These variations in the QD size introduce an inhomogeneous broadening of the absorption lines. Accordingly, we have accounted for the inhomogeneous broadening arising due to the variations in the radii of the quantum dots. The average QD absorption coefficient is calculated by assuming a Gaussian probability distribution function similar to the one chosen by Wu *et al* [17].

The theoretical model as developed in this section can be successfully employed to study and compare the emission and absorption spectra of (i) an atom in a lossy cavity, (ii) a single quantum dot (SQD) in a lossy cavity and (iii) a single quantum dot in an IQD. We have obtained results for strong-coupling ($g_e \gg \gamma_c, \kappa$) and weak-coupling ($g_e \ll \gamma_c, \kappa$) regimes.

3. Results and discussion

Optical confinement in a QD may be achieved by cleaving the substrate along the crystal planes. In GaAs, QDs have been formed naturally by interface steps in narrow quantum wells (QWs) [27]. Under certain circumstances, owing to the high gain in the active region, resonator facets are uncoated and yield a reflectivity of about 30% [11]. However, Weisbuch *et al* [4] as well as Lyngnes *et al* [10] have used microcavities having 98% and 99.5% reflectivity, respectively. In the former case, the coupling of the QD with the cavity field is weak as compared to the losses incurred in the cavity ($g \ll \kappa + \Gamma$) and is referred to as the weak-coupling limit (WCL). The other [4, 10] regime corresponds to the strong-coupling limit (SCL), where the coupling is strong as compared to the losses ($g \gg \kappa + \Gamma$).

A numerical analysis has been carried out for a system of small QDs of (i) CdS, of dimensions 19 Å [28], and (ii) GaAs/GaAlAs, of dimensions 56 Å [12]. The other material parameters for CdS and GaAs are given in table 1. The QDs are assumed to be irradiated by resonant lasers. The results for both strong- and weak-coupling limits are presented below.

Table 1. Material parameters of GaAs and CdS quantum dots.

						SCL			WCL	
Sample	R (nm)	a_B (nm)	ω_g (eV)	E_R (meV)	κ ($\times\omega_g$)	γ ($\times\omega_g$)	g ($\times\omega_g$)	κ ($\times\omega_g$)	γ ($\times\omega_g$)	g ($\times\omega_g$)
CdS	1.9[a]	2.9[b]	2.56[a]	28[c]	0.02[d]	0.001[e]	0.19[f]	0.7[g]	0.01[e]	0.19[f]
GaAs	5.6[h]	10.9[i]	1.514[i]	5.43[c]	0.02[d]	0.001[e]	0.29[f]	0.7[g]	0.01[e]	0.29[f]

[a] Reference [28].
[b] Reference [13].
[c] Calculated from the definition $E_R = \hbar^2/(2m_r a_B^2)$.
[d] Reference [4].
[e] Incorporated phenomenologically.
[f] Calculated from the expression $g_e = \mu_e E/\hbar$ for $e = 1$.
[g] Reference [11].
[h] Reference [12].
[i] Reference [34].

3.1. The strong-coupling limit

In this limit, the photon leakage κ is related to the transmittivity (T) of the cavity as $\kappa = \omega T$. Also considering $(\kappa - \Gamma)^2 \ll g_e^2$ and taking the inverse transform of (13), we get the real part

of ρ_{0e} as

$$\rho_{0e} = \sum_e \frac{g_e \Delta_e}{\alpha^2} \left[\sin^2(\alpha_e t/2) + \left(\frac{\sin \alpha_e t}{\alpha_e t} - 1 \right) (\kappa - \Gamma) t \right] \exp[-(\kappa + \Gamma) t] \tag{14}$$

with $\alpha_e = [\Delta_e^2 + 4g_e^2]^{1/2}$. ρ_{0e} obtained for strong QD–cavity coupling shows a superposition of three distinct forms. The first two of these oscillate at a frequency α_e, while the third gives a DC shift to ρ_{0e}. A careful examination of (14) clearly reveals that for small observation times ($t \ll \pi/\alpha_e$), the sine function contributes moderately to the DC factor, while for large observation times ($t > \pi/\alpha_e$), the DC factor dominates. However, the exponential decay of ρ_{0e} over time indicates that ρ_{0e} can be considered to be finite for times $t \leqslant (\kappa + \Gamma)^{-1}$. Thus the resultant ρ_{0e} is expected to exhibit an oscillatory exponential decay at the rate $\kappa + \Gamma$ and an oscillation frequency α_e. The values of Δ_e and g_e govern the magnitude of ρ_{0e}. The decay time can be enhanced by decreasing the values of $\kappa + \Gamma$. The expected nature of ρ_{0e}, as discussed, can be confirmed from a sample calculation. The various terms in equation (14) are plotted in figure 1 for a single value of e (=1). Curve a is obtained from the first term of (14) while curve b is obtained from the second term. Curve c represents ρ_{0e} as calculated from the complete expression for ρ_{0e} as defined in (14). Curve a clearly indicates a sine-squared variation superposed on an exponentially decaying function while curve b shows a superposition of a sine function and an exponentially decaying function. For small times, the sine-squared function makes a large contribution, while for large times the second term has a dominant role as is evident from curve c.

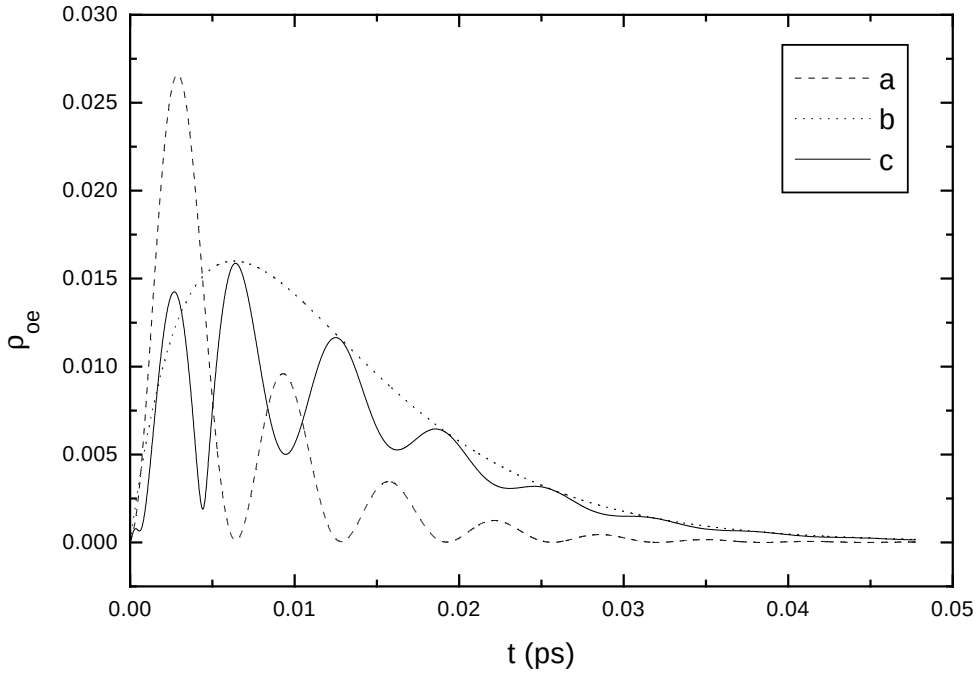

Figure 1. Sample calculations of ρ_{0e} (equation (14)) versus time. Curve a represents the first term in the square brackets in (14) while curve b is obtained from the second term of the same equation. Curve c was calculated from the complete expression.

In order to compare the nature of the emission spectra obtained for a quantum dot with that of the spectra of an atomic system in the microcavity, we have analysed the behaviour of ρ_{0e}

as a function of time by taking into account (i) only the 1s excitonic state and (ii) the transition from the ground state $|0\rangle$ to all of the $|e\rangle$ states. In the former case, the situation becomes similar to a simple two-level system exhibited by an atom. In the forthcoming discussions, case (i) has been denoted by the term 'representative atom'.

Figures 2(a) and 2(b) illustrate the time variation of ρ_{0e} obtained for realistic values of CdS and GaAs quantum dots of radius 19 Å and 56 Å, respectively. The two curves in each part are obtained for the representative atom and for a quantum dot. The oscillatorily decaying nature of ρ_{0e} is evident from both of the curves. The magnitude of ρ_{0e} is increased for the quantum dots as compared to that for the representative atom. This can be attributed to the fact that in the present model the QD has been represented as a combination of different excitonic levels $|e\rangle$. Thus contributions from each excitonic level add up to yield a larger value. These contributions are shown individually in the inset of the figure. Lyngnes *et al* [10] have studied the response of a semiconductor microcavity to a single intense femtosecond laser pulse. Their measurements of the upconversion intensity in an InGaAs QW placed within a Bragg mirror of reflectivity 99.6% exhibit similar behaviour. Although the experiment of Lyngnes *et al* [10] was performed on two QWs, in our opinion such experiments could be extended to a QD sample grown naturally from interface steps in narrow QWs [27].

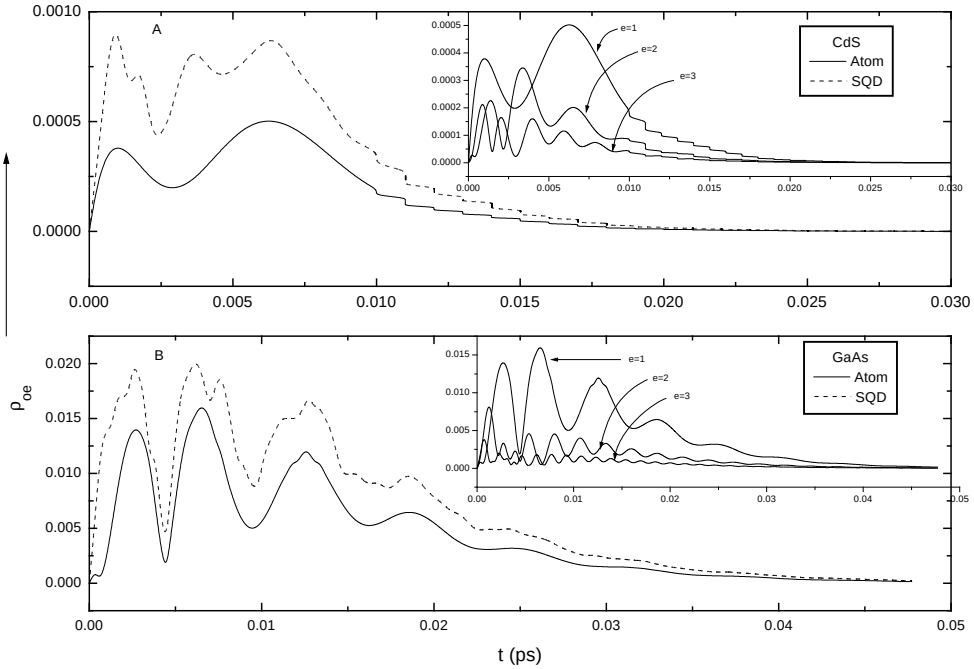

Figure 2. The temporal variation of ρ_{0e} in the strong-coupling limit, for CdS and GaAs quantum dots.

In a QD–microcavity experiment, it is difficult to isolate a single quantum dot of such small dimensions. Hence it is common practice to use an inhomogeneous distribution of QDs in the microcavity experiments. In an IQD the variation in size of the quantum dot causes a distribution of the energies. The inhomogeneous broadening may be taken into account by assuming that the particles have a Gaussian size distribution $F(R)$ around a mean value $\Delta R = xR_0$, with x being the percentage variation in the Gaussian width [17, 29]. Hence, the

average value of ρ_{0e} for a single QD in an array of many QDs may be defined, in a manner comparable to the approach of Wu *et al* [17], as

$$\rho_{0e}\big|_{av} = \int_0^{a_B} F(R)\rho_{0e}\big|_R \,\mathrm{d}R \tag{15}$$

where

$$F(R) = (\Delta R)^{-1}\sqrt{\ln 2/\pi}\,\exp\left[-\ln 2\,[(R - R_0)/\Delta R]^2\right].$$

The present formulations have been developed for a small quantum dot of dimension $R \leqslant a_B$; hence the limit of integration is selected for all possible sizes in the range $R = 0$ to a_B.

In figures 3(a) and 3(b), the temporal nature of the strong-coupling limit has been plotted for small QDs of CdS and GaAs, respectively, for different widths of the Gaussian size distributions. The solid curves were obtained for a single quantum dot taking into account the four excitonic states. The dashed curves were obtained for the average value of ρ_{0e} as given by $\rho_{0e}|_{av}$ with a Gaussian size distribution, having width $x = 20\%$. It is evident from the curves that the incorporation of a dot size distribution function broadens the curves. Also, for such distribution widths the small peaks collapse to a single broadened peak.

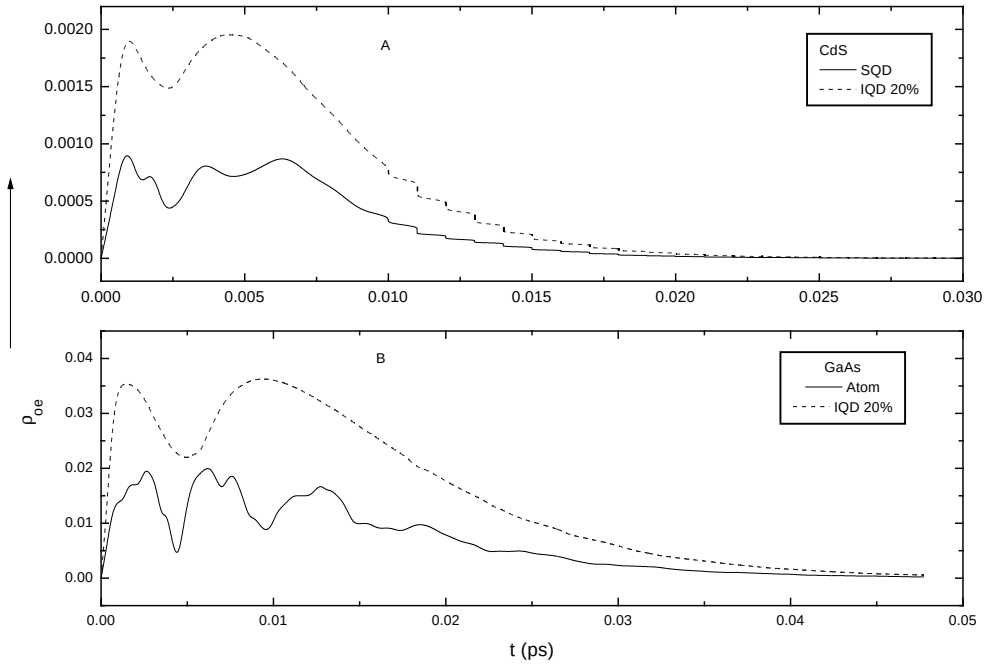

Figure 3. The time dependence of ρ_{0e} in the strong-coupling limit, for CdS and GaAs quantum dots.

3.2. The weak-coupling limit

In a low-Q cavity experiment, the relaxation mechanisms dominate over the coupling mechanism. Thus, to account for such realistic situations, we obtain ρ_{0e} for $(\kappa + \Gamma)^2 \gg g_e^2$. Taking the inverse transform of (13) we find

$$\rho_{0e} = \sum_e \frac{g_e}{\Delta_e + \mathrm{i}(\kappa + \Gamma)}\left[\exp(-2\Gamma t) - \exp[(\mathrm{i}\Delta_e - \kappa - \Gamma)t]\right]. \tag{16}$$

Equation (16) comprises an exponentially decaying (at the rate 2Γ) term superposed upon an oscillatory decay (at the rate $\kappa + \Gamma$) term. For $\kappa > \Gamma$, the oscillatory term will decay faster and one may not obtain the oscillations in the transmitted signal. On the other hand, for $\kappa \ll \Gamma$, an oscillatorily decaying output is expected. For the numerical estimates obtained for QDs of CdS and GaAs in the WCL, we have taken $\kappa = 0.7$ and $\Gamma = 0.01$. The other material parameters are chosen to be same as those used to obtain figures 2 and 3. As we have taken $\kappa \gg \Gamma$, the oscillatory term is found to decay faster in comparison with the first term in (16). This analytical feature can be verified from figure 4, where we have plotted the variation of ρ_{0e} as a function of time. The analytical results have been plotted for a representative atom (solid), for a SQD (dashed) and for an IQD (dotted). The amplitude of the oscillations in ρ_{0e} is found to be minimum in the case of an atom; it is reduced for a SQD and an IQD. A comparison of ρ_{0e} in the strong- and weak-coupling limits can also be made from figures 2 to 4. It can be seen that ρ_{0e} decays faster for the WCL as compared with the SCL.

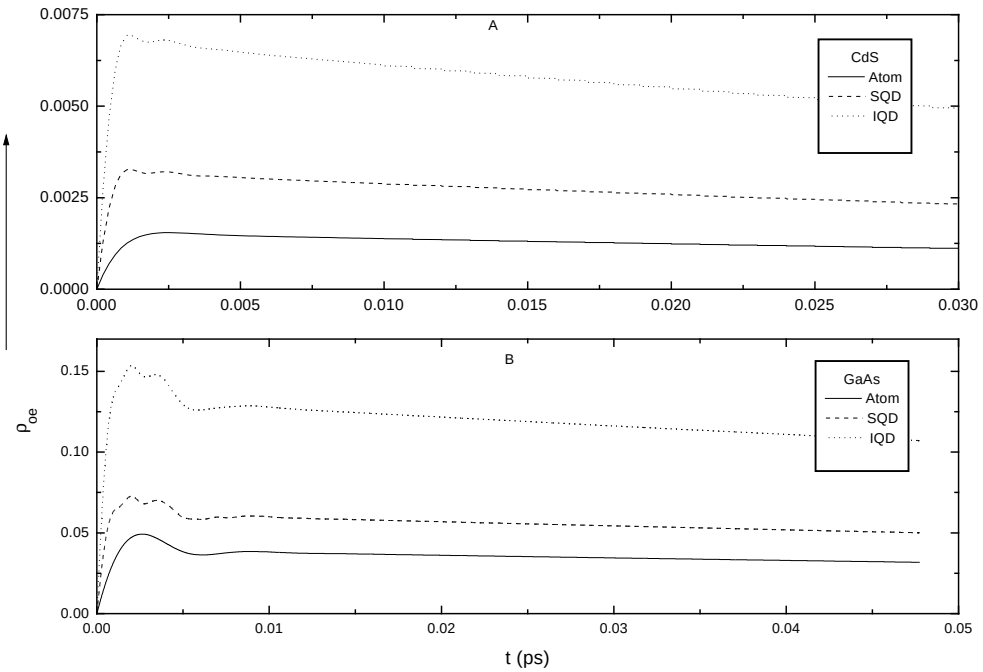

Figure 4. The variation of ρ_{0e} with time t in the weak-coupling limit, for CdS and GaAs quantum dots.

The experimental realization of the strong-coupling regime mentioned here is achieved in high-Q cavities described by large Bragg mirror reflectivities (≈95%) where the dot–photon coupling can be assumed to be strong. On the other hand, the weak-coupling regime mentioned here resembles more the practical situations where the cavity concept for the QD is not used and one observes the free-space response of a QD at high excitation densities, as in photoluminescence (PL) and absorption spectra studies of the QDs. In connection with this we can phenomenologically compare the results exhibited in figure 4 with the ones obtained by Heitz *et al* (their figure 8) [30] while studying the excited-state energy relaxation in stacked InAs/GaAs quantum dots.

4. The absorption spectrum

In order to observe the absorption spectrum, we adopt the standard technique for a medium saturated by an intense driving field. We assume that the system is weakly perturbed by a monochromatic probe field at a frequency ν such that the absorption characteristics can be monitored. The density matrix equation (1) will be modified in the presence of a weak probe field of the form

$$\frac{\partial \rho}{\partial t} = L\rho - \mathrm{i}\sum_e [G_e \pi_{e0}^{+} \exp(-\mathrm{i}\nu t) + \mathrm{h.c.}, \rho]. \tag{17}$$

Here, G_e couples the weak probe field with the system under observation. The exact solution of ρ can be obtained by expanding it in a series as

$$\rho = \rho^{(0)} + \rho^{(1)} + \rho^{(2)} + \cdots \tag{18}$$

with

$$L\rho^{(0)} = 0. \tag{19}$$

The first-order density matrix now yields

$$\rho^{(1)}(t) = -\mathrm{i}\int_0^t \exp[L(t-\tau)] \sum_e [G_e \pi_{e0}^{+} \exp(-\mathrm{i}\nu t) + \mathrm{h.c.}, \rho^{(0)}(\tau)]\, \mathrm{d}\tau. \tag{20}$$

The vacuum field of the pump modifies the probability of occupation of the quantum states. This in turn affects the absorption of the probe field. The time-average rate of absorption (W) of an atom in a cavity can be obtained by defining

$$W = \sum_e \frac{\mathrm{d}}{\mathrm{d}t}\langle P \rangle E' = -\mathrm{i}\nu \sum_e (\mu_{e0} E')\langle \pi_{e0}^{+} \rangle \exp(-\mathrm{i}\nu t) + \mathrm{c.c.} \tag{21}$$

where E' and μ_{e0} are the electric field amplitude of the probe field and the transition dipole moment, respectively. Following the procedure adopted by Agarwal and Puri [25], the time-average rate of absorption is found to be

$$W = 2\nu \sum_e \left[\left[\frac{|\mu_{e0} E'|}{\hbar} \right]^2 \mathrm{Re}\left[\frac{1}{r_e^{+} - r_e^{-}} \left[\frac{r_e^{+} - \mathrm{i}\omega + \kappa}{\mathrm{i}\nu - r_e^{+}} - \frac{r_e^{-} - \mathrm{i}\omega + \kappa}{\mathrm{i}\nu - r_e^{-}} \right] \right] \right] \tag{22}$$

where $r_e^{\pm}$ are defined via (10). The time-average rate of absorption obtained in (22) clearly indicates resonances at two complex frequencies $r_e^{\pm}$ with the probe field at frequency ν. Carmichael *et al* [24] have used master equations to study the emission spectra of an atom in a lossy cavity. In the present section, we have confined our attention to the absorption spectra of the semiconductor QD. Agarwal and Puri [25] obtained a doublet structure in both the emission and absorption spectra for an atom coupled to the cavity. Eberly and Wodkiewicz [31] drew the inference that the doublet structure in the spontaneous emission could be observed only when the atom is in resonance with the cavity mode. For a given energy state, the present formulation can be easily reduced to that of an atom in a cavity. The doublet structure of the absorption spectrum as obtainable from (22) would demonstrate two peaks separated by $\Delta_e/2 + g_e$. The incorporation of the expression of $r_e^{\pm}$ as given by (10) makes (22) cumbersome for analytical investigations. Therefore, we have simplified (10) for the special cases of the strong- and weak-coupling limits under resonant situations such that $\Delta_e \simeq \Gamma$. However, the numerical estimates have been made by incorporating (10) and taking into account the special conditions, namely $\Delta_e \ll \Gamma$ and $\Delta_e \gg \Gamma$.

4.1. The strong-coupling limit

The dynamics of the absorption spectrum in the SCL may be understood by recalling the expressions for $r_e^{\pm}$ at $\Delta_e \simeq \Gamma$ as

$$r_e^{\pm} = \mathrm{i}\left(\omega + \frac{\Delta_e}{2} \pm g_e\right) - \frac{\kappa + \Gamma}{2}. \tag{23}$$

It is transparently obvious from (22) that the absorption spectrum will show a doublet structure and the two resonant peaks will occur at $\nu = \omega + \Delta_e/2 \pm g_e$, the separation between the two peaks being $2g_e$. Also, the width of each peak is totally controlled by the relaxation parameters κ, γ and γ_c. All of the relaxation constants incorporated in the basic equation of motion contribute to the additive nature of the spectral width in the absorption spectrum. For larger values of relaxation parameters in the SCL, one can expect the doublet structure to merge to a singlet structure, showing that the resolution of the two lines depends upon the damping constants. The rate of absorption has been numerically calculated for the CdS and GaAs QDs using the same parameters as were chosen for obtaining figures 2 and 3. The probe frequency dependence of the time rate of absorption has been plotted in figures 5(a) and 5(b) for CdS and GaAs quantum dots, respectively. The dotted and solid curves represent a single QD and an atom. The figure depicts symmetric curves for positive and negative probe detuning. The absorption spectrum obtained for the atomic system shows a single doublet structure, while the spectrum obtained for a QD exhibits discrete doublet lines characteristic of different excitonic states. Thompson *et al* [32] have experimentally observed the normal-mode splitting from an atom–cavity system. A solid-state analogue of such an effect has been reported by Weisbuch *et al* [4] where the cavity field was in resonance with the excitonic levels of the quantum

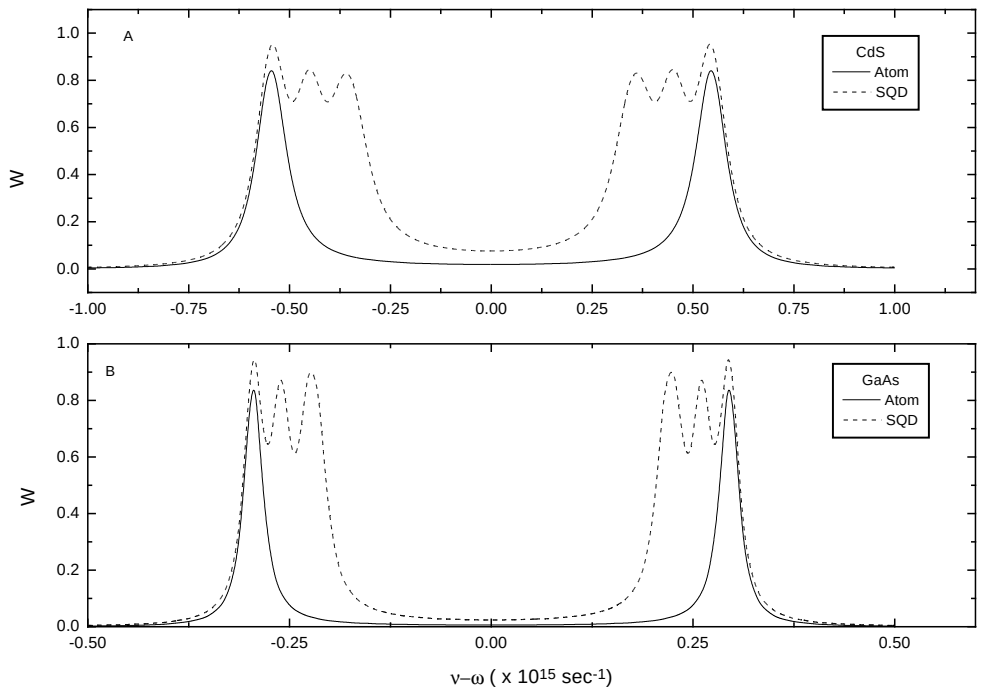

Figure 5. The absorption spectrum as a function of the pump–probe detuning parameter in the strong-coupling limit, for CdS and GaAs QDs.

well. Strong exciton–photon coupling has also been reported by Houdre *et al* [5], where they concluded that the splitting depends on the exciton oscillatory strength. They have compared the experimental observations with the linear dispersion model. Jahnke *et al* [33] performed cw pump–probe measurements of the excitonic normal-mode coupling in a microcavity. The results have been obtained for the strong-coupling as well as the weak-coupling regime of cavity-enhanced emission. The theoretical results obtained by us are qualitatively similar to the ones reported in the above-mentioned observations [5, 33].

In order to demonstrate the effect of inhomogeneous broadening arising due to the variation of QD sizes in an array of quantum dots, we have incorporated a Gaussian size distribution through the definition

$$W_{av} = \int_0^{a_B} W F(R)\, \mathrm{d}R.$$

The rate of absorption has been plotted as a function of the detuning parameter in figures 6(a) and 6(b) for the QDs of CdS and GaAs, respectively. The solid curves are obtained for single quantum dots, of finite sizes 19 Å and 56 Å, while the dashed curves are obtained for an IQD of average radius distribution having 20% width.

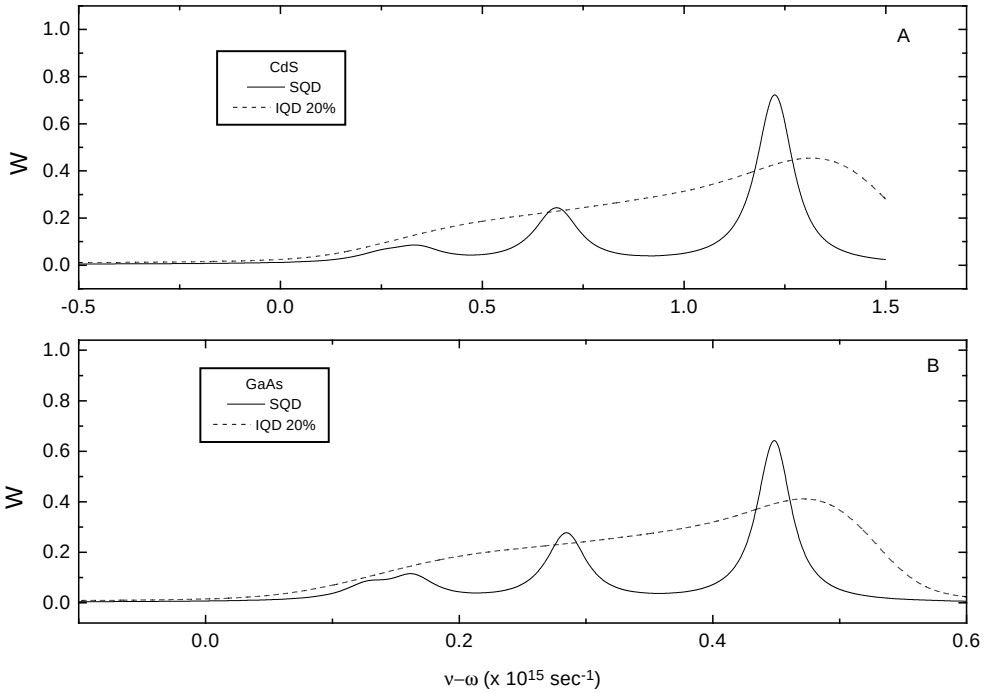

Figure 6. The dependence of the absorption spectrum on the pump–probe detuning in the strong-coupling limit, for CdS and GaAs crystals.

4.2. The weak-coupling limit

In the weak-coupling limit and near-resonance situation ($\Delta_e \simeq \Gamma$), equation (10) reduces to

$$r_e^+ = \mathrm{i}(\omega + \Delta_e) - \Gamma \qquad \text{and} \qquad r_e^- = \mathrm{i}\omega - \kappa. \tag{24}$$

The use of (24) in (22) yields the time-average rate of absorption as

$$W = 2\nu \sum_e \left[\frac{|\mu_{e0}E'|}{\hbar}\right]^2 \left[\frac{\Gamma}{(\nu-\omega-\Delta_e)^2+\Gamma^2}\right]. \tag{25}$$

Equation (25) clearly indicates a single resonant peak at $\omega + \Delta_e = \nu$. Also, the absorption spectrum will be a Lorentzian having a width of Γ. Hence, splitting of the absorption spectrum will not be expected in the weak-coupling limit where the cavity and system losses dominate over the semiconductor–microcavity coupling parameter g_e. The linewidth of the spectrum in the present case will be completely decided by the system relaxation parameters γ and γ_c. The variation of W as a function of the detuning parameter $(\omega - \nu)$ has been plotted in figure 7 for realistic cases of CdS and GaAs QDs in the microcavity. Again, for a specific value of $e = 1$ the two-level system is represented and one obtains the single peak exhibited by the solid curve. The amplitude of the peak increases for a SQD of finite size as shown by the dashed curve, and further increase in the peak value can be seen for an IQD via the dotted curve.

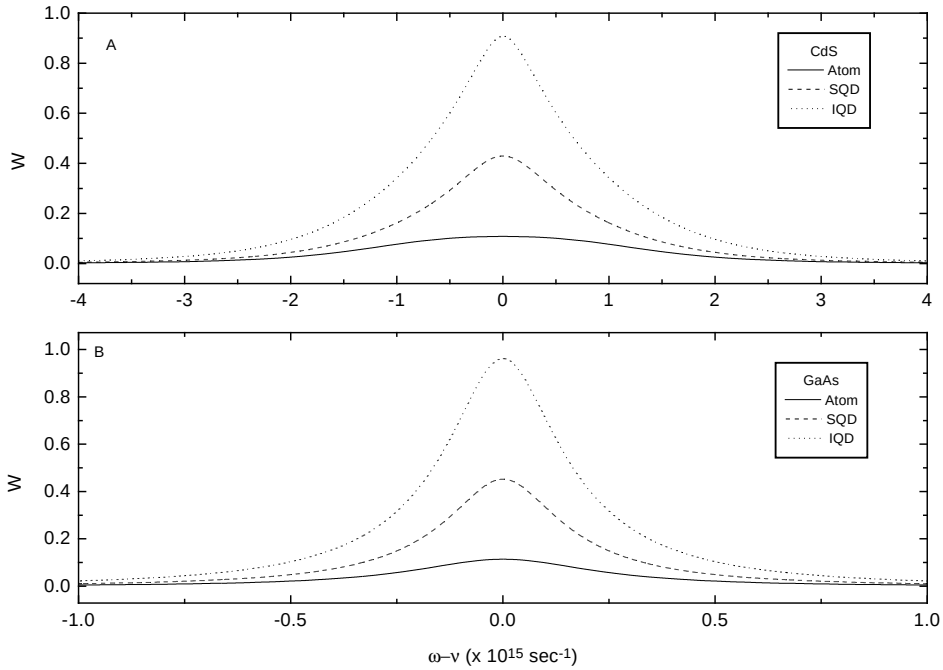

Figure 7. The variation of the absorption spectrum with probe detuning in the weak-coupling limit, for CdS and GaAs quantum dots.

5. Conclusions

In conclusion, we have developed a theoretical model for studying the cavity photon–quantum dot coupling by taking into account the different excitonic levels. The sample calculations are made for quantum dots of CdS and GaAs in both strong- and weak-coupling limits. The temporal behaviours demonstrated for ρ_{0e} are found to be similar to the observations of time-resolved measurements for QDs [10, 30]. In the strong-coupling regime, the solid-state analogue of vacuum Rabi splitting is observed. In the weak-coupling regime, the doublet structure disappears.

Acknowledgments

The authors are very grateful to Professor Pranay K Sen and Dr K C Rustagi for fruitful discussions. The financial support from the University Grants Commission (PS), Council of Scientific and Industrial Research (JTA), New Delhi, and the Department of Atomic Energy, Mumbai, is gratefully acknowledged.

References

[1] Yamamoto Y and Slusher R E 1993 *Phys. Today* **28** (June) 66
[2] Haroche S and Kleppner D 1989 *Phys. Today* **24** (January) 24
[3] Morin S E, Wu Q and Mossberg T W 1992 *Opt. Photonics News* (August) 9
[4] Weisbuch C, Nishioka M, Ishikawa A and Arakawa Y 1992 *Phys. Rev. Lett.* **69** 3314
[5] Houdre R, Stanley R P, Oesterle U, Ilegems M and Weisbuch W 1994 *Phys. Rev.* B **49** 16 761
Houdre R, Stanley R P, Oesterle U, Ilegems M and Weisbuch W 1994 *Phys. Rev. Lett.* **73** 2043
[6] Kireev A N and Dupertuis M A 1996 *Opt. Commun.* **123** 268
[7] Hopefield J J 1958 *Phys. Rev.* **112** 1555
[8] Blockelmann U, Roussignol Rh, Filoramo A, Heller W, Abstreiter G, Brunner K, Bohm G and Weimann G 1996 *Phys. Rev. Lett.* **76** 3622
[9] Savona V, Andreani L C, Schwendimann P and Quattropani A 1995 *Solid State Commun.* **93** 733
[10] Lyngnes O, Berger J D, Prineas J P, Park S, Khitrova G, Gibbs H M, Jahnke F, Kira M and Koch S W 1997 *Solid State Commun.* **104** 297
[11] Chow W W, Koch S W and Sargent M III 1994 *Semiconductor Laser Physics* (Berlin: Springer) pp 8, 9
[12] Schmitt-Rink S, Miller D A B and Chemla D S 1987 *Phys. Rev.* B **35** 8113
[13] Banyai L and Koch S W 1993 *Semiconductor Quantum Dots* (Singapore: World Scientific) p 122
[14] Haug H 1988 *Optical Nonlinearities and Instabilities in Semiconductors* ed H Haug (Boston, MA: Academic) pp 53–80
[15] Hanamura E 1987 *Solid State Commun.* **62** 463.
[16] Hu Y Z, Lindberg M and Koch S W 1990 *Phys. Rev.* B **42** 1713
[17] Wu W, Schulman J N, Hsu T and Efron G 1987 *Appl. Phys. Lett.* **51** 710
[18] Beenakker C W J 1991 *Phys. Rev.* B **44** 1646
Beenakker C W J, van Houten V and Staring A A M 1991 *Phys. Rev.* B **44** 1657
[19] Jalabert R A, Stone A D and Alhassid Y 1992 *Phys. Rev. Lett.* **68** 3468
[20] Blick R H, van der Weide D W, Haug R J and Ebert K 1998 *Phys. Rev. Lett.* **81** 689
[21] Folk J H, Patel S R, Godijin S F, Huibers A G, Cronenwett S M, Marcus C M, Campman K and Gossard A C 1996 *Phys. Rev. Lett.* **76** 1699
[22] Patel S R, Cronenwett S M, Stewart D R, Huibers A G, Marcus C M, Duruoz C I, Harris J S Jr, Campman K and Gossard A C 1998 *Phys. Rev. Lett.* **80** 4522
[23] Gorelik L Y 1998 *Phys. Rev. Lett.* **80** 4526
[24] Carmichael H J, Brecha R J, Raizeu M G, Kimble H J and Rice P-R 1989 *Phys. Rev.* A **46** 5516
[25] Agarwal G S 1974 *Quantum Statistical Theories of Spontaneous Emission and their Relation to Other Approaches (Springer Tracts in Modern Physics 70)* ed G Hohler (Berlin: Springer)
[26] Obernettinger F and Badii L 1973 *Tables of Laplace Transforms* (Berlin: Springer)
[27] Gammon D, Snow E S, Shanabrook B V, Katzer D S and Park D 1996 *Phys. Rev. Lett.* **76** 3005
[28] Butty J, Peyghambarian N, Kao Y K and Mackenzie J D 1996 *Appl. Phys. Lett.* **69** 3224
[29] Peyghambarian N, Koch S W and Mysrowicz A 1993 *Introduction to Semiconductor Optics* (Englewood Cliffs, NJ: Prentice-Hall) pp 270–86
[30] Heitz R, Kalburge A, Xie Q, Grundmann M, Chen P, Hoffmann A, Madhukar A and Bimberg D 1998 *Phys. Rev.* B **57** 9050
[31] Eberly J H and Wodkiewicz K 1977 *J. Opt. Soc. Am.* **67** 1252
[32] Thompson R J, Rempe G and Kimble H J 1992 *Phys. Rev. Lett.* **68** 1132
[33] Jahnke F, Kira M, Koch S W, Khitrova G, Lindmark E K, Nelson T R Jr, Wick D V, Berger J D, Lyngnes O, Gibbs H M and Tai K 1996 *Phys. Rev. Lett.* **77** 5257
[34] Lotti R C and Andreani L C 1997 *Phys. Rev.* B **56** 3922